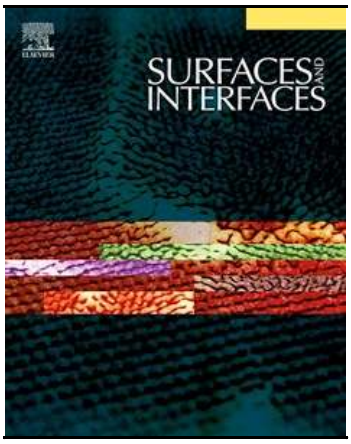

On the Evolution of Stresses due to Lattice Misfit at a Ni-superalloy and YSZ Interface

Abir Bhattacharyya , David Maurice

PII: S2468-0230(18)30259-1
DOI: 10.1016/j.surfin.2018.05.007
Reference: SURFIN 207

To appear in: *Surfaces and Interfaces*

Received date: 12 September 2017
Revised date: 25 April 2018
Accepted date: 6 May 2018

Please cite this article as: Abir Bhattacharyya , David Maurice , On the Evolution of Stresses due to Lattice Misfit at a Ni-superalloy and YSZ Interface , *Surfaces and Interfaces* (2018), doi: 10.1016/j.surfin.2018.05.007

On the Evolution of Stresses due to Lattice Misfit at a Ni-superalloy and YSZ Interface

Abir Bhattacharyya* and David Maurice

U.S. Department of Energy, National Energy Technology Laboratory, 1450 Queen Ave SW, Albany, OR 97321, USA

Abstract

The principle of elastic strain energy minimization is used to predict the possible ranges of allowable lattice misfit for the formation of coherent and semi-coherent interfaces between a Ni superalloy substrate and a cubic yttria stabilized zirconia (c-YSZ) ceramic coating. Depending upon the elastic modulus, failure strength in compression and tension, and the Burgers vector of the film material, the magnitude of allowable lattice misfit can vary over a wide range. It is shown that compressive stresses as high as several gigapascals may exist at the coherent YSZ films, and a higher positive lattice misfit can sometimes be more favorable for the formation of a semi-coherent interface than is a lower negative lattice misfit. Both coherency and the effect of lattice misfit on the interfacial stress decrease with an increase in the thickness of the film. The effect of lattice misfit on the evolution of interfacial stresses during film deposition must be considered during the design of dissimilar materials interfaces and for the prediction of interfacial delamination and the fracture of films.

Keywords: Thermal barrier coating, lattice misfit, thermal mismatch, metal-ceramic interface, coherent, semi-coherent interface.

1. Introduction

Metal-ceramic multilayered structures are frequently used in electronic devices [1, 2] , solid oxide fuel cells [3] and thermal barrier coatings (TBC) etc. [4]. The bonding between metal and ceramic interfaces is important in the context of thermal barrier coatings (TBC), which are made of refractory materials of low thermal conductivities and are used to protect the metallic base components from high temperature [5-7], and from erosive and corrosive atmospheres [8, 9] . The TBCs used in turbine blades may need thicknesses up to several hundreds of microns depending upon the required reduction in temperature from the coating surface to the substrate. Multilayered TBCs with each layer thickness of a few tens of nanometers are also being deposited on thin metal foils [10] as these multilayered TBCs can enhance the thermal resistance via interfaces and hence can improve the performance of TBCs. The mechanical integrity of all these structures depend on the properties of the metal-ceramic interfaces [4, 11].

The fabrication of strong metal-ceramic interface is challenging due to the differences in bonding characteristics, surface energies, lattice parameters, thermal expansion coefficients, individual material strength and toughness of metals and ceramic materials, and low interfacial toughness [12]. These interfaces are subjected to various stresses during the deposition process. Thermally induced stresses are generated at the interface between the film and the substrate upon cooling during film deposition due to differences in the coefficient of thermal expansion (CTE) between the substrate and the film [13-15]. During heteroepitaxial growth of a film, a difference in lattice parameters (i.e. lattice misfit) between dissimilar materials can also strain the film which may influence the integrity of the interface. The thermal mismatch stress can be reduced by selecting film and substrate materials with similar coefficients of thermal expansion (CTE). The difference in CTE being high for ceramic-metal interfaces, often functionally graded (FG)

cermet layers are deposited to reduce the thermal mismatch among the layers. However, lattice misfit among the FG layers still exist. Appropriate alloying or doping can be used to tailor the lattice parameter of film and substrate to reduce the lattice misfit induced stress. Therefore, by proper selection of alloying elements, and by varying the degree of alloying over the thickness of a coating, it is possible gradually reduce the lattice misfit and thermal mismatch induced stresses between the deposited layers and can reduce stresses at dissimilar interfaces.

Several analytical and numerical models have been developed to predict interfacial stresses in uniform and FG coatings due to thermal mismatch [14-18]. But the effect of lattice misfit on the evolution of stresses in film, defect generation at the interface, and their consequence to interfacial adhesion are not well studied. The lattice misfit may contribute significantly to the stresses in films if the thickness is of submicron scale and hence important for multilayered or FG coatings. Typically films can grow pseudomorphically when the lattice misfit is small [19]. It is reported that a coherent interface can form when the lattice misfit is less than ~10% [19-21]. These reports are mostly based on observations made using transmission electron microscopy [21, 22]. However, the actual lattice misfit for each film-substrate system is different, and the allowable lattice misfit (limit) for the pseudomorphic film growth of a given film-substrate system is neither well defined nor previously been predicted. Beyond this limiting lattice misfit for pseudomorphic growth, the lattice parameter mismatch cannot be accommodated by the elastic lattice strain alone, and dislocations nucleate at the interface to relieve the interfacial strain. Therefore, questions arise as to how to estimate the maximum allowable lattice misfit for a coherent interface in a film-substrate bi-material system, and how does the lattice misfit influence the defect nucleation and degree of coherency of a substrate-thin film system?

Several experimental methods have been proposed to estimate the residual stresses induced by lattice misfit and thermal mismatches and to investigate the stress release by dislocations. These include using beam curvature [23], Raman spectroscopy [24, 25] and X-ray diffraction [26]. However, the experimental methods cannot distinguish the individual contribution by the thermal mismatches and lattice misfit to the total stress and do not account for any stress relaxation due to lattice defects.

In an effort to address these questions, we first describe a minimization of elastic strain energy based analytical methodology to predict the nucleation of dislocations and nature of interfaces for any hypothetical lattice misfit that may exist at any hypothetical interface between cubic YSZ (c-YSZ) and a Ni based superalloy. The c-YSZ-Ni superalloy interface is commercially important due to its extensive use as a TBC in turbine engines. Allowable lattice misfits for the formation of coherent and semi-coherent interfaces are predicted based on macroscopic mechanical properties. This model has been used to predict the nature of interfaces and stresses in the film and the substrate for real c-YSZ-Ni interfaces. The orientation relationships between c-YSZ and Ni available in literature are selected to introduce a microscopic description of the interface in the macroscopic model. The contribution of stresses arising due to thermal mismatch and the lattice misfit are predicted along with the evolution of stresses with film thickness. The effects of thermal mismatch, lattice misfit and film thickness on the evolution of interfacial stress and defects are key to the selection of materials for TBC systems.

2. *Theoretical Development*

2.1 Lattice misfit and mismatch strain at the interface

The lattice misfit between two dissimilar crystals of a film-substrate system is expressed as [27]:

$$f = \frac{a_f - a_s}{a_s} \quad (1)$$

Where a_s and a_f are the lattice parameters of the substrate and the film, respectively. Typically, a film deposited on a substrate will be in compression if the lattice parameter of the film is greater than that of the substrate, and vice versa. According to this definition of lattice misfit, the film is in compression if $f > 0$ or in tension if $f < 0$, and the lattice misfit and strain due to mismatch (or mismatch strain) are opposite in sign. The lattice misfit strongly depends on the lattice orientation at the interface. For example, in a two-dimensional (x-y) cubic YSZ-Ni interface, the magnitude of misfit (*f*) for facet $(111)_{c-YSZ} // (1\bar{1}1)_{Ni}$ in the x-direction will be different from that of the facet $(2\bar{2}0)_{c-YSZ} // (022)_{Ni}$ oriented in the y-direction. Therefore, it is necessary to know the orientation relationship between the film and the substrate at the interface for calculating the lattice misfit (f).

An interface can be coherent, semi-coherent or incoherent depending upon the lattice misfit at the interface. Schematics of various types of interfaces are shown in Fig. 1. Coherent interfaces typically form when the lattice misfits are < ±10% [20]. Such interfaces can be strained or unstrained based on the magnitude of lattice mismatch at the interface (Fig. 1(a) and 1(b)). Semi-coherent interfaces (Fig. 1(c)) form for a lattice misfit of < 20% during hetero- epitaxial growth of a material having a different crystal structure and bonding characteristics (for e.g. metal and ceramic)[20]. The high mismatch cannot be accommodated by elastic strain alone at the lattices at the interface. Consequently, dislocations form at the interface to relieve the

strain due to misfit as defined in Eq. (1). Misfits beyond 20% result in the formation of an incoherent interface (Fig. 1(d)) and thus 20% can be considered as a practical limit of the lattice misfit (f) contributing to the strain at the interface. For a full or partial epitaxy, the lattices within the film and the substrate at the vicinity of a coherent or semi-coherent interface will orient themselves to reduce the lattice misfit (f) to less than 20%.

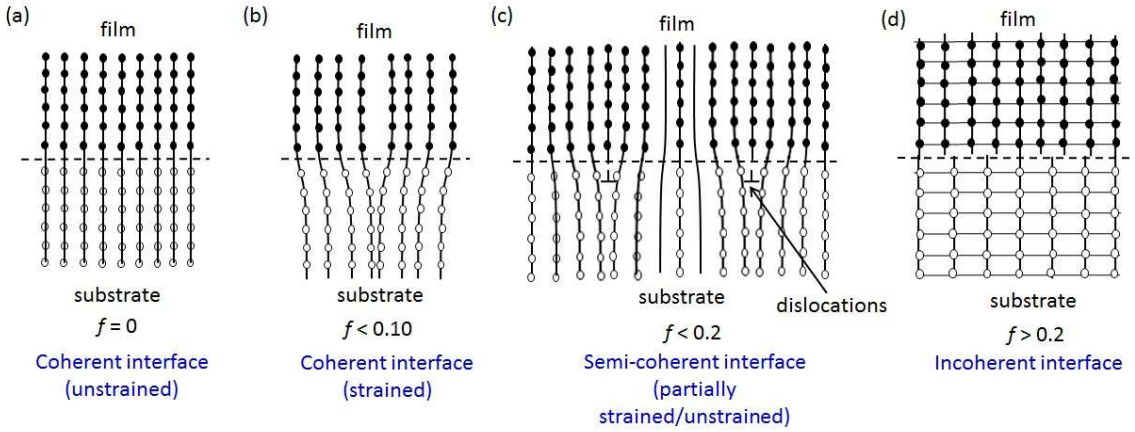

Figure 1: Schematics of different types of interfaces between dissimilar film and substrate. (a) unstrained coherent interface, (b) strained coherent interface, (b) semi-coherent interface with dislocations, (d) incoherent interface.

For epitaxial growth in a substrate-film system, a limiting misfit (f^{Lim}) for the coherent interface can be defined beyond which a semi-coherent interface will form. Accordingly, a mean strain ($|\varepsilon_m| \le |f|$) at the interface of a film-substrate system can be defined as [27]

$$\varepsilon_m = \begin{cases} -f & \text{for } f \le f^{Lim} \\ -\left(f + \frac{b}{p}\right) = -\left(\frac{a - a_s}{a_s} + \frac{b}{p}\right) & \text{for } f > f^{Lim} \end{cases} \qquad (2)$$

Where b is the Burgers vector of a dislocation and p is the mean spacing between dislocations in a square array of dislocations. Eq. (2) suggests that a positive f results in negative mean strain (ε_m) and vice versa. The mean dislocation spacing p is directly related to the dislocation density (N) by $N = 1/p^2$ [28, 29].

For a low lattice misfit ($f < f^{Lim}$) a coherent interface forms and the entire magnitude of f contributes to the interfacial strain ε_m (or stress), i.e. $\varepsilon_m = f$ (see Eq. (2)). For $f < f^{Lim}$ dislocation formation will not take place, however, the stresses due to the lattice misfit remain in the interface. The biaxial stress arising from the lattice misfit is given by $\sigma = 2\mu \frac{(1+\nu)}{(1-\nu)} f$, which contributes to the elastic strain energy per unit area according to $W = 2\mu \frac{(1+\nu)}{(1-\nu)} f^2 h$, where μ, ν and h represent the shear modulus, Poisson's ratio and thickness of the film, respectively. The elastic strain energy of the film increases with increase in the lattice misfit and thickness of the film. Eventually for $f > f^{Lim}$ and beyond a critical film thickness (h_c), dislocation nucleation at the interface becomes favorable as the dislocations reduce the mean strain according to $\varepsilon_m = f - b/p$ (see Eq. (2)). The corresponding biaxial stress due the lattice misfit after the nucleation of dislocation is also reduced, $\sigma = 2\mu \frac{(1+\nu)}{(1-\nu)} (f - b/p)$. Hence the elastic strain energy of the film is expected to be lower than a dislocation free interface for same lattice misfit value favoring the nucleation of dislocations. Consequently, the interface will have a high dislocation density, but the stress at the interface may be very low due to dislocation

nucleation induced strain relief.

2.2 Equilibrium dislocation density at an interface

Equation (2) and the discussion in the previous section implies that dislocations nucleate at the interface when the lattice misfit $f > f^{Lim}$. The signs of f and b_p will always be opposite as dislocations relieve the lattice misfit. As a result, the magnitude of mean strain will always be less than or equal to the lattice misfit, i.e. $|\varepsilon_m| \leq |f|$. However, the magnitude and sign of ε_m depends on the relative magnitudes and sign of f and b_p. Determination of p is therefore necessary.

The methodology to determine p is adopted from an analysis by Willis *et al*. [30] who developed a theory for an infinite two-dimensional array of regularly spaced dislocations. The total elastic strain energy per unit area (W_T / L^2) of a substrate-film system can be calculated in terms of the lattice misfit, f. According to the definition of f (Eq. (1)), the film is in compression when the lattice misfit is negative. The total elastic energy per unit area can be decomposed into two components according to:

$$\frac{W_T}{L^2} = W_1 + W_2 = 2\mu \frac{1+\nu}{1-\nu} \varepsilon_m^2 h + \frac{2}{p} E_{DS} \qquad (3)$$

The first term (W_1) is the elastic strain energy per unit area due to the mean strain arising from the lattice mismatch in the layer, which is partially relaxed by the formation of dislocations according to Eq. (2), and the second component (W_2) represents the contribution from the self- energy (E_{DS}) of dislocations. Here h is the thickness of the film. The self-energy of dislocations, E_{DS} is expressed as:

$$= \quad \mu b^2 \quad \left\{ \left[\frac{p}{} \left(- \quad ^{-s} \right) \right] + \frac{s e^{-s}}{} - 1 \quad s^2 e^{-s} \quad - \right.$$

$$E_{DS} \quad \frac{}{4\pi(1-\nu)} \left\{ \ln \left[2\pi b \quad 1 \quad e \quad \right] \right. \quad 1 - e^{-s} \quad 2 \left(1 - e^{-s}\right)^2 \quad \left. 1 \right\} \qquad (4)$$

Where b is the Burgers vector and

$$s = \frac{4\pi h}{p} \qquad (5)$$

The E_{DS} in Eq. (4) considers interactions between the dislocations and thus represents an improvement over existing models [31, 32]. A limitation of the model described above is that as it uses linear elasticity theory to calculate energy, it breaks down at the core of the dislocation line, which is usually within a radius of $\approx b$ according to Jain [27].

Equilibrium spacing (p_{EQ}) between the dislocations can be achieved by minimizing the total energy ($W_T \left| \frac{2}{L} \right.$). Based on Eq. (3) W_1 increases with increasing misfit strain and thickness of the film. The minimization of total energy ($W_T \left| \frac{2}{L} \right.$) is therefore governed by the self-energy (E_{DS}) of dislocations. The dislocation spacing for a strain-free film (p_{SF}) can be obtained from Eq. (2) after substituting $\varepsilon_m = 0$. Therefore, for a stress-free semi-coherent film $W_1 = 0$, which is also the minimum value of W_1 (Eq. (3)).

3. Results and Discussion

Materials for a representative TBC system were selected to evaluate the model described in section 2. Ni-based alloys are typically used for high-temperature applications such as furnace tubes,

turbine blades, heat shields etc. [33]. Therefore, a NiCoCrAlY alloy (Inconel 738) is used as the substrate or base material for model testing. Cubic Yttria stabilized zirconia (c-YSZ), a widely-used TBC is chosen as the top coat material for testing this model.

3.1 Effect of lattice misfit on dislocation nucleation

The energy components W_1, W_2 and the total elastic energy ($W_T L^2$) are normalized with $\frac{\mu}{2\pi(1-\nu)}$ and are plotted as a function of p for high ($f = -0.15$) and low ($f = -0.002$) lattice misfits as shown in Fig. 2. The equilibrium configuration of a dislocation array for a given film thickness is determined by minimizing the total elastic strain energy ($W_T L^2$) with respect to the dislocation separation distance (p). It is evident from Fig. 2(a) that for a low lattice misfit ($\varepsilon_{m_{f_{i,i+1}}} = -0.002$), the total energy varies only asymptotically with p and energy minimization does not take place for the atomically thin film (h = 1 nm, Fig. 2(a)). This suggests that nucleation of dislocations is not favorable at such a small thickness of the film. However, the energy minimization occurs at a greater film thickness (h = 50 nm, Fig. 2(b)) at which dislocation nucleation becomes favorable. In this case the minimum $W_T L_2$ occurs at a higher p value than the p value for which W_1 is minimum. This suggests that the equilibrium dislocation spacing, p_{EQ} is greater than the dislocation spacing at the strain-free interface (p_{SF}), i.e. $p_{EQ} > p_{SF} = b/f$. The value of p_{SF} can be determined by substituting $\varepsilon_m = 0$ in Eq. (2) However, with further increases in thickness equilibrium and strain (stress)-free dislocation spacing converges again and eventually $p_{EQ} \approx p_{SF}$.

In contrast, for a high lattice misfit, the minimum $W_T L_2$ occurs at a lower p value than

the p value for which W_1 is minimum (Fig. 2(c)). The equilibrium dislocation spacing, p_{EQ} is smaller than the dislocation spacing at the strain-free interface (p_{SF}), i.e. $p_{EQ} < p_{SF} = b/f$.

For high lattice misfits, the equilibrium dislocation spacing (p_{EQ}) is very low (Fig. 2(c)) and results in an extremely high equilibrium misfit dislocation density (N_{EQ}) that is greater than the dislocation density for a strain free interface ($N_{SF} = (f\ |b)^2$), i.e. $N_{EQ} > (f\ b)^2$. This reveals that the stress in the film may reverse its sign as the misfit increases from low to high magnitude. But with further increases in thickness the difference between the equilibrium and strain (stress)-free dislocation spacing decreases and eventually $p_{EQ} \approx p_{SF}$ (Fig. 2(d)). Reversal of the sign of stress at high lattice misfits was reported by Moridi et al. [34]. His study showed that the stress state at the interface between silicon and sapphire changes from compressive to tensile with decreasing spacing between the dislocations. The dislocation energy term (W_2) decreases with decreasing dislocation spacing (p) and converges to $-\infty$ at $p = 0$. Such variation is unrealistic as there will be an overlap of dislocation cores below a certain value of p after which Eq. (3) and (4) cannot be used [27]. This core cut-off value is assumed to be $2.5b \approx 0.9nm$ and is typical of the dislocation core radius for metals and ceramics.

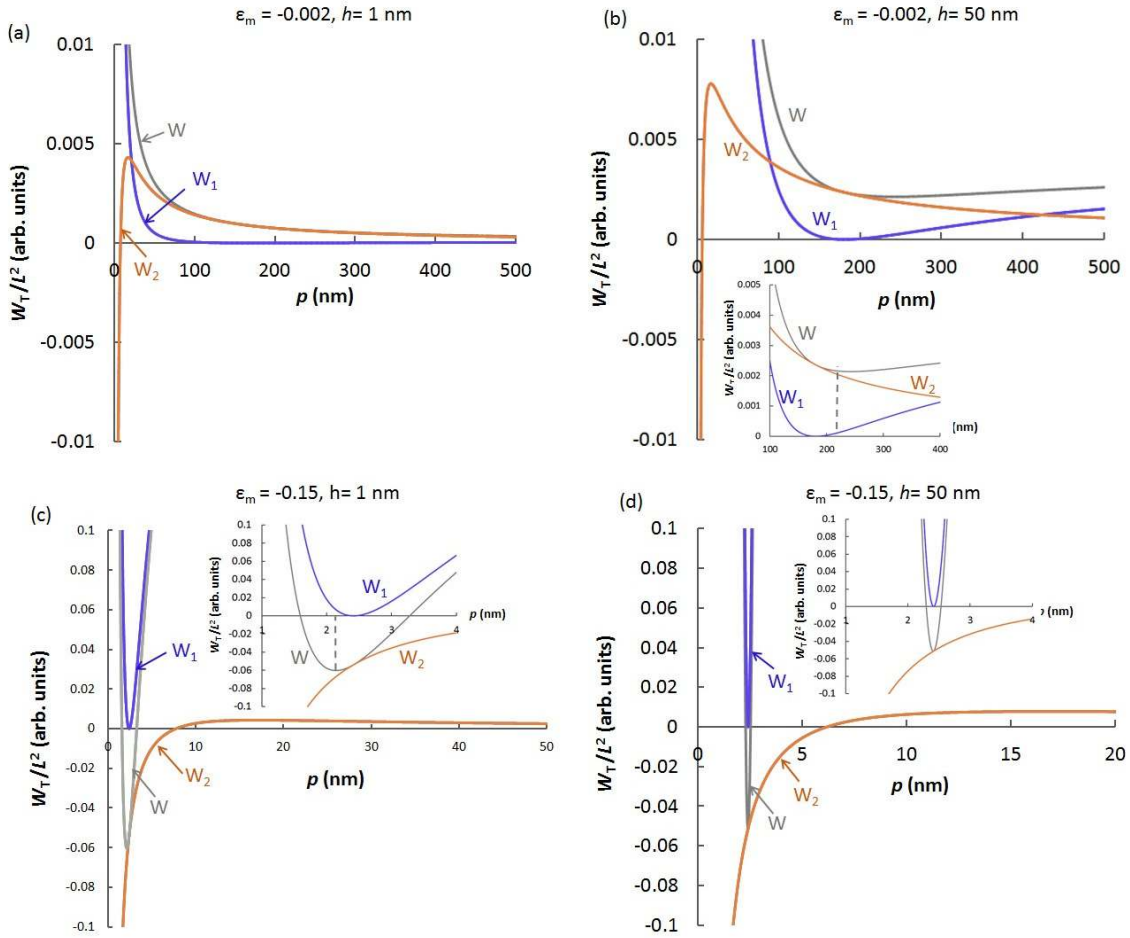

Figure 2: Elastic strain energy associated with the formation of interfacial dislocations as a function of dislocation spacing for two hypothetical cases of lattice misfit (a) for $\varepsilon_{mf_{i,i+1}} = -0.15$, $h = 1\ nm$, (b) for $\varepsilon_{mf_{i,i+1}} = -0.15$, $h = 50\ nm$, (c) for $\varepsilon_{mf_{i,i+1}} = -0.002$, $h = 1\ nm$, (d) for $\varepsilon_{mf_{i,i+1}} = -0.002$, $h = 50\ nm$. The Burger's vector $= \frac{a}{2}[110] = 0.362$ nm for the cubic-YSZ crystals. The insets of Fig. (b) and (c) show that the dislocation spacing for a stress-free interface (p_{SF}, when $W_1 = 0$) is different from that for an equilibrium interface (p_{EQ}, when $W = 0$). For low lattice misfits $p_{SF} < p_{EQ}$, whereas, for high lattice misfits $p_{SF} > p_{EQ}$. The inset of Fig. (d) shows that p_{SF} and p_{EQ} tends to converge at higher film thicknesses.

The equilibrium misfit dislocation densities (N_{EQ}) for several lattice misfits were calculated from the p value by $N_{EQ} = 1/p_{EQ}^2$ and are plotted as a function of film thickness in Fig. 3 for low and high lattice misfits. For the lower values of lattice misfit, no dislocations form below a critical film thickness (h_c) (Fig. 1(d)). This behavior is a reflection of the asymptotic behavior of $\frac{W_T}{L^2}$ vs. p plot for small lattice misfits for small film thickness (Fig. 1(a)). Therefore, a coherent strain can exist within the film below a critical film thickness (h_c). Dislocations nucleate at a film thickness greater than h_c and the strain at the interface is consequently reduced.

The critical film thickness (h_c) for dislocation nucleation varies with the lattice misfit (*f*). The increasing critical thickness for dislocation nucleation with decreasing lattice misfit (i.e. $h_{c1} > h_{c2} > h_{c3}$) indicates the greater tendency towards formation of a coherent interface at lower lattice misfits during the epitaxial growth of the film. The value of h_c is typically a few to tens of nanometers and is a strong function of the lattice misfit. Above this critical thickness, the strain energy stored in the film due to lattice mismatch causes the generation of misfit dislocations which relieve the interfacial strain/stress at the expense of reduced interface adhesion [35].

The remaining mean strain within the film in the vicinity of the interface after the formation of misfit dislocations is expressed in Eq. (2). The equilibrium dislocation density (N_{EQ}) increases (or p_{EQ} decreases) with the thickness of the film (Fig. 2(a)) and eventually saturates to a value corresponding to that of a stress-free interface (i.e. $N_{SF} = (f\ b)^2$). For lattice misfits of

the order of f = -0.15 and -0.10, dislocations readily nucleate at the interface and the equilibrium

dislocation density is on the order of $\approx 10^{17} / m^2$, which is significantly high for ceramics and even for highly deformed metals. Such a high dislocation density can reduce the adhesion of the interface and may lead to interfacial cracking. In contrast to low lattice misfits, for high lattice misfits the dislocation density reduces with increasing film thickness and eventually becomes equal to that of a strain-free interface ($N_{SF} = (fb)^{-2}$).

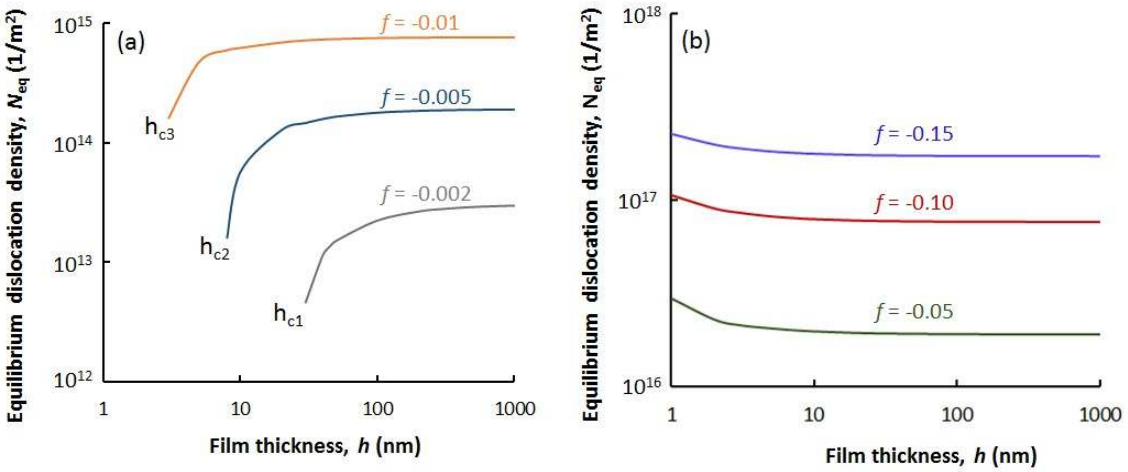

Figure 3: Evolution of equilibrium dislocation density as a function of film thickness in Ni-cubic YSZ film-substrate system for hypothetical cases of lattice misfits. (a) for three low lattice misfit values, (b) for three high lattice misfit values.

3.2 Prediction of allowable lattice misfit for coherent interface and degree of coherency

The macroscopic failure strength of a material can be used to predict the maximum allowable mean strain at an interface ε_m^{Lim}. A positive (film in compression) or negative (film in tension) misfit can occur at the interface depending upon the lattice orientation of the substrate and the film at the interface. The corresponding mean strain (ε_m) can therefore be either negative, positive or zero depending upon the sign and magnitude of lattice misfit (f), the

magnitude of f^{Lim}, the Burgers vector (b) and the dislocation spacing (p) or density (N) at the interface. In an x-y interface, we assume that the lattice constants can relax in the z-direction. The biaxial stress in the film arising from the mean strain due to the lattice misfit at an interface is calculated from [19],

$$\sigma_m = \frac{E}{1-\nu}\varepsilon_m \qquad (6)$$

Here E and ν are Young's modulus and Poisson's ratio of the film material, respectively, and $E = 2\mu(1+\nu)$ where μ is the shear modulus. The maximum allowable stress in the film (σ_{mf}^{Lim}) is limited by the fracture strength (ε_{Fail}^{T} and ε_{Fail}^{C} for tension and compression, respectively) of the film. The maximum allowable mean strain at the interface (ε_{m}^{Lim}) can therefore be calculated from Eq. (6) by substituting the value of the fracture strength for (σ_m). However, the considerable difference in the fracture strengths of the ceramics under tension and compression results in significantly different values of allowable mean strains ($\varepsilon^{Lim})_m$ for compression and dilatation of the lattice of the film material.

The hardness of 95-98% dense YSZ is reported to be 11-13.5 GPa [36, 37]. The corresponding compressive strength (σ_c) is determined to be 3.67-4.5 GPa using Tabor's rule [38] ($\sigma_c = H/3$, where H is the Vickers hardness of the material). Considering the compressive and flexural tensile strengths of YSZ to be 4.66 GPa and 300 MPa [39], respectively at room temperatures, we obtain the maximum allowable mean strain (ε_m^{Lim}) at the interface to be $\varepsilon_{fail}^{C} = -0.018$ and $\varepsilon^{fail} = 0.0012$ for the contraction and dilatation of the YSZ lattice. Clearly a

large compression-tension asymmetry is evident in the allowable mean strain at any interface comprised on at least one side with a ceramic.

Based on the values of ε_m^{Lim} from Eq. (6) and the elastic energy minimization criteria described in section 2.2, it is possible to calculate the limiting lattice misfits for coherent (i.e. f^{Lim}) and semi-coherent interfaces. As the strain energy model described in section 2.2 breaks down at a length scale on the same order of the magnitude as the core radius of dislocation ($\approx b$ [27]), we assume the smallest film thickness of 1 nm. Therefore we postulate that the limiting lattice misfit (f^{Lim}) for a fully coherent interface should correspond to the maximum lattice misfit for which total energy minimization just occurs at $h = 1\ nm$ (i.e. $W_T\ L$ vs. $|f|$ response remains asymptotic). A coherent interface then forms when $|f| \le |f^{Lim}|$ and the interface is subjected to a constant stress of $Ef/(1-\nu)$. For the structural integrity of the film, the coherency strain must be smaller than the failure strain of the film.

Strain energy minimization and the asymmetry in compressive and tensile failure strengths of cubic YSZ leads to $f^{Lim} = 0.0146$ and -0.0012 for a film subjected to compression and tension, respectively. Interface characteristics for the YSZ-Ni system for a range of lattice misfit values are described in Table 1. The mean strain at the interface immediately after deposition (i.e. $h = 1\ nm$) depends strongly on the magnitude and sign of the lattice misfit.

Table 1: Interface characteristics of a 1 nm thick cubic YSZ film on Ni substrate for a range of lattice misfits

Misfit	**Dislocation density**	**Mean Strain (ε_m)**	**Interface characteristics**
$f < -0.0986$	$N_{EQ} >> N_{SF}$	$\varepsilon_m > \varepsilon_{fail}^{C}$	Semi coherent interface with high dislocation density expected to result in

			fracture of film under compressive stress.
$-0.0986 \le f \le -0.0213$	$N_{EQ} > N_{SF}$	$\lvert\varepsilon_m\rvert < \lvert\varepsilon^C_{fail}\rvert$	Stressed semi-coherent interface, the film under compression.
$-0.0213 \le f \le -0.0203$	$N_{EQ} < N_{SF}$	$\lvert\varepsilon_m\rvert < \lvert\varepsilon^T_{fail}\rvert$	Stressed semi-coherent interface, the film under tension.
$-0.0203 \le f \le -0.0146$	$N_{EQ} << N_{SF}$	$\lvert\varepsilon_m\rvert > \lvert\varepsilon^T_{fail}\rvert$	Film expected to rupture under tension despite dislocation nucleation
$-0.0146 \le f \le -0.0012$	NA	$\lvert\varepsilon_m\rvert = \lvert f \rvert > \lvert\varepsilon^T_{fail}\rvert$	Film expected to rupture under tension without dislocation nucleation
$-0.0012 > f \le 0.0146$	NA	$\varepsilon_m = f$	Stressed coherent interface (in tension when $f < 0$ and in compression when $f > 0$)
$0.0146 < f \le 0.0213$	$N_{EQ} < N_{SF}$	$\lvert\varepsilon_m\rvert < \lvert\varepsilon^C_{fail}\rvert$	Stressed semi-coherent interface, the film under compression.
$0.0213 < f \le 0.0228$	$N_{EQ} > N_{SF}$	$\lvert\varepsilon_m\rvert < \lvert\varepsilon^T_{fail}\rvert$	Stressed semi-coherent interface, the film under tension.
$f > 0.0228$	$N_{EQ} >> N_{SF}$	$\lvert\varepsilon_m\rvert > \lvert\varepsilon^T_{fail}\rvert$	Semi coherent interface with high dislocation density expected to result in fracture of film under tensile stress.

A fully coherent 1 nm thick film forms when -0.0012 < f ≤ 0.0146 (see Table 1). Such a small lattice misfit ensures structural integrity of a 1 nm thick film. For 0.0146 < f < 0.0213, dislocations are expected to readily nucleate at the interface as soon as deposition begins (h = 1 *nm*) and a semi-coherent interface forms. In this case $N_{EQ} < N_{SF}$ and hence some compressive strain remains in the film even after dislocation nucleation. Dislocation nucleation is not energetically favorable based on the strain energy minimization for

$-0.0146 \le f \le -0.0012$ and a coherent interface is predicted. However, the coherent interface is expected to fail by rupture of the film due to high tensile stress as $|\varepsilon_m| > |\varepsilon^T_{Fail}|$.

Although dislocation nucleation is energetically favorable for $-0.0203 \le f \le -0.0146$, the film is expected to rupture under tensile stress since the lower density of equilibrium dislocations (i.e. $N_{EQ} << N_{SF}$) is insufficient to relieve the lattice misfit strain at the interface. Interestingly, a sufficient number of dislocations are present at a higher negative lattice misfit for $-0.0213 \le f \le -0.0203$ and allow a semi-coherent interface stressed under compression, to form. For the cases of $-0.0986 \le f \le -0.0213$ and $0.0213 < f \le 0.0228$, high dislocation densities are achieved, and the interface is stressed in compression and tension, respectively. The change of the sign of the strain (stress) occurs due to high lattice misfit as described in the previous section. Beyond the lattice misfit of 0.0228 and -0.0986, the equilibrium dislocation densities are significantly higher than the N_{SF}, and the films may be expected to fail under tension and compression, respectively.

3.3 Stresses at a cubic YSZ-Ni interface

The crystal structure of 8 mol% -YSZ is cubic (CaF_2 type) and we assume that the crystal structure of the Ni-based bond coat material is FCC [40]. The interfaces are usually composed of low index planes and are thus expected to have low energies. Therefore, orientation relationships (OR) between the low index planes of cubic YSZ (c-YSZ) and Ni (or FCC-Fe, which has a comparable lattice parameter to the bond coat and Ni) are considered to calculate the lattice misfits at the interface between the top coat and the bond coat. The preferred orientation

relationship requires that the interfacial energy should be minimized during the formation of an

interface, which is achieved by matching the close packed planes and directions of the two crystals that minimize the lattice mismatch at the interface. This leads to the minimization of interfacial energy. In the current study, we have selected ORs reported in literature. Christensen *et al.* [41] and Sasaki *et al.* [42] have reported possible ORs at the interface between c-YSZ and Ni based on first principle calculations and experimental observations using high resolution transmission electron microscopy (HRTEM). Dickey et al. [43] studied Ni/YSZ interfaces fabricated by molecular beam epitaxy, using electron diffraction technique, and determined the predominant orientation relationship)(Table 2). Heo et al. [44] obtained Ni/YSZ specimen by Ni re-deposition onto YSZ (001) from the ion milling of Ni. Poklad *et al.* [22] reported ORs at the interface between cubic ZrO_2 and FCC-Fe, which has same crystal structure and similar lattice parameter to Ni. The various possible ORs between c-YSZ and Ni are listed in Table 2.

Table 2: Orientation relationships between c-YSZ-Ni and c-YSZ-FCC Fe available in literature.

Orientation Relationship (OR)	Methods Used	References
$(111)_{c-YSZ} // (111)_{Ni}$, $[\bar{1}10]_{c-YSZ} // [\bar{1}10]_{Ni}$	TEM, Electron diffraction	Sasaki *et al*. [42]
$(001)_{c-YSZ} // (111)_{Ni}$, $[110]_{c-YSZ} // [110]_{Ni}$	TEM	Heo *et al.* [44]
$(100)_{c-ZrO_2} // (111)_{Ni}$, $[010]_{c-ZrO_2} // \lfloor \bar{1}10 \rfloor_{Ni}$,	Scanning TEM (STEM)	Dickey *et al*.[43]
$(111)_{c-YSZ} // (111)_{\gamma-Fe}$, $[211]_{c-YSZ} // [\bar{0}11]_{\gamma-Fe}$ $(111)_{c-YSZ} // (\bar{1}\bar{1}\bar{1})_{Ni}$, $[211]_{c-YSZ} // [\bar{0}11]_{Ni}$	TEM, Density functional theory (DFT)	Poklad *et al*., Christensen *et al.* [41]
$(001)_{c-YSZ} // (001)_{Ni}$,$[010]_{c-YSZ} // [110]_{Ni}$	Coincidence of reciprocal lattice points (CLRP)	Sasaki *et al*. [42]

These ORs along with various possible commensurability ratios (CR) between the crystal lattices are used to calculate the lattice misfits at the interfaces. The CR is defined as the integral multiple of lattice parameter or interplanar spacing required to match at the interface. As we

selected a NiCoCrAlY based Inconel alloy as our substrate, and c-YSZ as the coating, their respective lattice parameters (see Table 4) are used to calculate the lattice misfit values reported in Table 3. From the calculated lattice misfit, we can predict the nature of the interface based on the methodology described in section 3.2. Among all the ORs listed in Table 2, only one representative case for each type of interface is listed in Table 3 along with the respective lattice misfit value.

Table 3: Representative orientation relationships (OR) for interfaces between c-YSZ-Ni and c-YSZ-FCC Fe as reported in literature. The same ORs are considered to estimate the lattice misfits between c-YSZ and a NiCoCrAlY base alloy in this study.

Interface types	Orientation Relationship (OR)	Commensurability Ratio (CR)	Misfit (*f*)	References
Incoherent (case i)	$(111)_{c-YSZ} // (111)_{MCrAlY}$ $[\bar{1}10]_{c-YSZ} // [\bar{1}10]_{MCrAlY}$	1:1	0.42	Sasaki *et al*. [42]
Semi-coherent (case ii)	$(\bar{1}11)_{c-YSZ} // (\bar{1}11)_{MCrAlY}$ $[2\bar{1}\bar{1}]_{c-YSZ} // [0\bar{1}1]_{MCrAlY}$	5:4	0.0264	Christensen *et al.* [41]
Coherent (case iii)	$(001)_{c-YSZ} // (001)_{MCrAlY}$ $[010]_{c-YSZ} // [\bar{1}10]_{MCrAlY}$	1:2	0.0057	Sasaki *et al*. [42]

For example, the lattice misfit (*f*) for the incoherent interface (case (i) in Table 2) is calculated from Eq. (7) based on the interplanar spacings (d) of the lattice planes that are perpendicular to the interface.

$$f = \frac{d_f - d_s}{d_s} \tag{7}$$

Where d_s and d_f are interplanar spacing of the substrate and film (bond coat and c-YSZ in this case), respectively.

The $(1\bar{1}0)$ plane is perpendicular to the (111) plane and therefore the interplanar spacings of $(1\bar{1}0)$ planes are used to calculate the misfits for the $[1\bar{1}0]_{c-YSZ}$ // $[1\bar{1}0]_{MCrAlY}$ OR (Table 2). This OR is equivalent to a cube on cube matching at the interface. For a 1:1 lattice CR between c- YSZ and NiCoCrAlY, the calculated misfit is 0.42 (Table 3). Similarly the lattice misfits for the other possible ORs are calculated and reported in Table 3. Among the three cases listed in Table 3, we test our model for the smallest lattice misfit (case iii) and determine the corresponding stress profile as a function of film thickness. The effect of lattice misfit and thermal mismatch on the evolution of stresses is described subsequently. For case (ii) the lattice misfit is mostly relieved due to the nucleation of dislocations. Whereas for the incoherent interface (Case (i)), the atomic structure and chemical bonds determine the stability of the interface and have not been considered in this study.

3.4 Residual stress after deposition

To show the effect of lattice misfit on the evolution of stresses at the interface we have considered a small initial lattice misfit of 0.0057 (case iii). A fully coherent interface exists for this misfit when $h < 7$ *nm* (based on Fig. 1) during the initial stage of the film deposition process (i.e. when film thickness is only a few atomic layers). Initially the film thickness is assumed to be 5 nm. Then we increase the film thickness and show how the stress profile evolves. The stress profile for the first case therefore considers the effects of both thermal mismatch strain and lattice misfit strain and the second case considers only the effect of thermal mismatch.

A schematic of the film-substrate system is shown in Fig. 4(a). Since the ceramic film and metal substrate mutually constrain each other, elastic strains will arise in both the film and

the substrate to meet the requirement of strain compatibility at the interface. The resulting compatibility equation becomes

$$\varepsilon_{sub}^{el} - \varepsilon_{film}^{el} = -\left(\varepsilon_{sub}^{Th} - \varepsilon_{film}^{Th}\right) - \varepsilon_m \qquad (8)$$

Where ε_{sub}^{el} and ε_{film}^{el} are elastic strains and ε_{sub}^{Th} and ε_{film}^{Th} are thermal strains in substrate and film, respectively. ε_m is the strain due to lattice misfit and is estimated from Eq. (2) for a given lattice misfit.

(a)

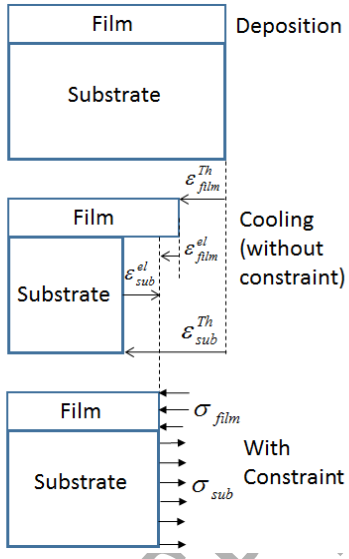

(b)

Layer	T (°C)	E (GPa)	ν	α (10^{-6} K^{-1})	a (A°)
8 mol% YSZ Film	20	204	0.10	9.68	5.12
	800	179	0.11	9.88	
	1000	186	0.12	10.34	
Inconel 738 Substrate	20	204	0.32	12.6	3.59
	800	161	0.34	15.4	
	1000	137	0.34	16.3	

Figure 4: (a) Schematic of a film-substrate system during deposition, cooling without constraint from substrate, and with constraint from substrate, (b) Material properties for cubic-YSZ film and Inconel 738 substrate.

The elastic strains for substrate and film are given as

$$\varepsilon^{el} = \frac{1-\nu_{sub}}{}\sigma \quad \text{and} \quad \varepsilon^{el} = \frac{1-\nu_{film}}{}\sigma \qquad (9)$$

$$E_{sub}^{sub} \quad E_{film}^{film}$$

Where σ_{sub} and σ_{film} are the equibiaxial stresses in the substrate and film, respectively.

The thermal strains for the substrate and film are expressed as

$$\varepsilon_{sub}^{Th} = \alpha_{sub}\Delta T \text{ and } \varepsilon_{film}^{Th} = \alpha_{film}\Delta T \tag{10}$$

Where α_{sub} and α_{film} are coefficient of thermal expansion of substrate and film, respectively.

To satisfy equilibrium condition, the summation of in-plane forces should be zero, i.e.

$$\sigma_{sub}h_{sub} + \sigma_{film}h_{film} = 0 \tag{11}$$

Here h_{sub} and h_{film} are the thicknesses of the substrate and film, respectively, and σ_{sub} and σ_{film} are the biaxial stresses in the substrate and film, respectively. Combining Eq. (8) and Eq. (11) the stress in the film and the substrate can be expressed as

$$\sigma_{film} = \frac{\Delta\alpha\Delta T + \varepsilon_m}{\left[\frac{1-\nu}{E}_{film} + \frac{1-\nu}{E}_{sub}\frac{h_{film}}{h_{sub}}\right]} \text{ and } \sigma_{sub} = \frac{-\left(\Delta\alpha\Delta T + \varepsilon_m\right)\frac{h_{film}}{h_{sub}}}{\left[\frac{1-\nu}{E}_{film} + \frac{1-\nu}{E}_{sub}\frac{h_{film}}{h_{sub}}\right]} \tag{12}$$

Where $\Delta\alpha = \alpha_{sub} - \alpha_{film}$ and for thin films $\left(h_{film} \middle| h_{sub}\right) << 1$ and $\sigma_{film} = \frac{E\Delta\alpha\Delta T + \varepsilon_m}{1-\nu}$.

$_{film}$

Equations (12) are used to plot the stress profiles through the TBC layer thickness. The temperature dependent mechanical and physical properties of the film and substrate material are provided in Fig. 4(b).

The calculations of stresses for this initial state were performed for a 5 nm thick top coat and 12.7 mm thick substrate. The equibiaxial stress distribution as a function of thickness of the TBC

layers is shown in Fig. 5(a) for cooling down from a deposition temperature of 1200°C to 20°C for mean misfit strain (ε_m) values of zero (case (ii)) and -0.0057 (case (iii) in Table 2), respectively, arising due to lattice misfit between the YSZ top coat and the IN 738-substrate.

Such a change in temperature is typical in chemical vapor deposition (CVD) and electron beam vapor deposition techniques.

Fig. 5(a) reveals that a moderate amount of compressive elastic stress (~ - 879 MPa) is generated within the YSZ top coat even when the mean lattice misfit strain at the interface is considered zero (blue solid line). This stress is generated only due to the difference in thermal expansion coefficients between the top coat and the bond coat materials during the cooling process. The amplitude of circumferential stress at the top coat and substrate interface increases to -2332 MPa (red dashed line) when a mean strain of -0.0057 due to the lattice misfit of $f = 0.0057$ between the top coat and substrate is included in the model (case (iii) in Table 2). The 5 nm thick ceramic top coat is highly stressed due to this small lattice misfit, and an under-prediction of film stress by almost 50% is therefore possible if we neglect the effect of lattice misfit. The error may even be higher if the temperature difference is lower and the effect of lattice mismatch strain dominates.

As the magnitude of the stress is lower than the fracture strength of YSZ (~ 4 GPa), this is not expected to cause cracking of the ceramic at the interface. However, the TBC is prone to failure by rupture of the film if subjected to external loading. The top coat is expected to be under compression since the coefficient of thermal expansion of the YSZ ceramic is smaller than that of the bond coat and the substrate. The elastic compressive residual stress counters any applied tensile stresses at the surface or subsurface regions within the top coat and thus enhances the life of the coating.

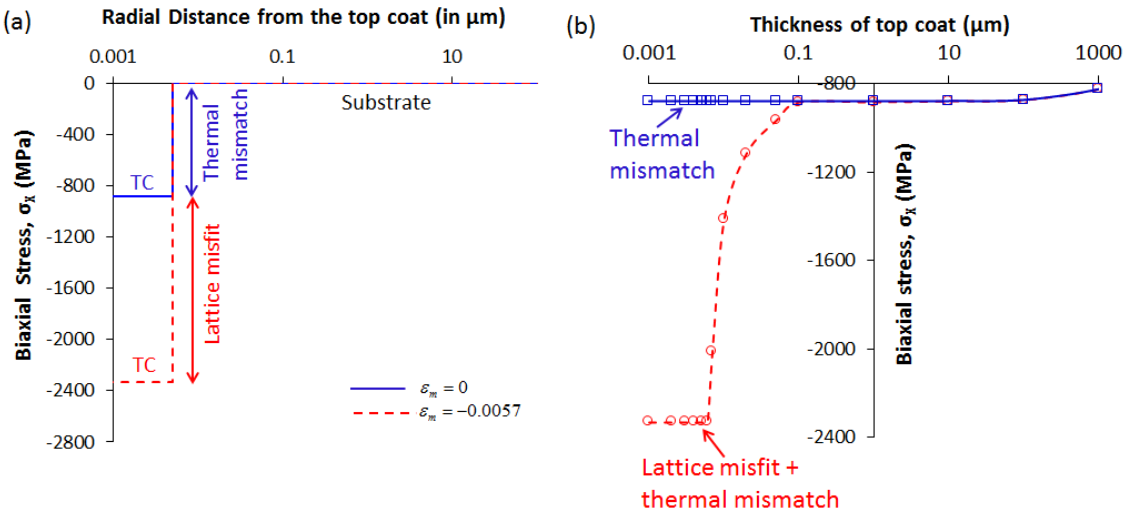

Figure 5: Biaxial stress profile due to cooling of a TBC system from 1200°C to 20°C during deposition. (a) Without considering the effect of lattice misfit strain ($\varepsilon_m = 0$, solid line) and considering the lattice misfit strain ($\varepsilon_m = -0.0057$, dashed line) between the top coat and Ni substrate. The thickness of the top coat = 5 nm, (b) Evolution of thin film stresses with increasing thickness of the film during deposition for $f = 0.0057$. The film is fully coherent up to the thickness of 5 nm. Dislocation nucleation occurs beyond this and the stress relaxes to a lower value. Only thermal stress remains at the interface beyond a film thickness of approximately 100 nm.

The effect of film thickness on the circumferential stress is shown in Fig. 5(b) for an initially coherent interface for the lattice misfit of 0.0057. The solid blue line shows the stress distribution due to the thermal mismatch only, whereas the red dashed line demonstrates the combined effect of lattice misfit and thermal mismatch. Clearly the lattice misfit contributes to the magnitude of stress significantly up to a film thickness of 100 nm. Beyond 100 nm, the predictions are nearly identical and the effect of lattice misfit on stress is negligible. However, dislocations evolve with increasing thickness and reduce the adhesion of the interface. Beyond a film thickness of approximately 200 μm, the high film-to-substrate thickness ratio causes the thin film assumption to break down, and the stress varies with the thickness as the thicker film strains

the substrate due to mismatch in elastic moduli. The resulting compressive stress in film is due to

the effect of thermal mismatch only. This was experimentally verified within the ceramic topcoat by Tanaka et al. [45] Using micro-Raman spectroscopy, they measured compressive residual stress in the range of ~ −200 MPa in a 4 mol % YSZ coating, which was deposited by EB-PVD. Using X-ray diffraction (XRD) and Raman spectroscopy, Teixeira *et al*. [46] measured compressive residual stress up to −250 MPa in plasma sprayed coatings. The low magnitude of compressive stress may be due to a lower deposition temperature and a lower Young's modulus for porous YSZ top coatthan the 203 GPa modulus used in our model for a fully dense cubic YSZ. Using synchrotron x-ray diffraction Li et al. [47] measured a nonlinear distribution of compressive residual stresses in the range between −200 MPa and −600 MPa within the top coat of a 8 wt% YSZ-NiCrAlY-Hastelloy TBC, and compared the magnitude with their analytical model, which predicted approximately 600 MPa of compressive stress uniformly distributed along the thickness of the top coat.

To render this theoretical residual stress calculation more tractable, we have used a flat interface based solely on the geometry of crystals. Real interfaces can be curved and wavy which might create additional stresses at the interface resulting from elastic interactions between the two materials. However, evolution of these stresses has been studied previously using analytical and finite element models which approximated the wavy interface as a sinusoidal profile [48]. The stress-states arising due to a curvy interface in the presence of a thermally grown oxide has also been studied [49]. Additional tensile and compressive stresses are induced within the top coat, TGO, and bond coat depending upon the curvature due to roughness [48-51]. Due to the sinusoidal interface geometry before the formation of a TGO, tensile stresses exist at hill locations in the TBC, whereas compressive stresses exist at the valley locations [49]. These

additional stresses due to the curved geometry of interfaces have not been considered in this study.

The model presented here can be applied to functionally graded TBCs that are manufactured to reduce the stress gradient among the individual layers. As observed from Fig. 5, the lattice misfit contributes to high levels of stresses in individual layers when the thickness of each graded layer is of submicron size. Our study further reveals that for a greater individual FG layer thicknesses, the lattice misfit stress is reduced via dislocation nucleation, which in turn reduces the interfacial adhesion. These must be accounted for to analyze the structural integrity of the FG TBCs. By varying the concentration of appropriate alloying elements, the composition of the coating as well as the substrate can be varied gradually to reduce the thermal and lattice mismatch gradient across the interfaces [52-54].

Although lattice misfit does not influence the stress distribution at higher film thickness, still it provides critical information about the interface formation at the beginning of deposition. Depending upon the elastic and physical properties of a material system, the lattice misfit may cause failure of the film during early stages of deposition. Therefore, consideration of lattice misfit is important for material selections and the design for TBC systems.

4. Conclusions

A methodology to estimate the allowable lattice misfits for coherent and semi-coherent interfaces for a cubic YSZ-Ni based superalloy film-substrate system is provided. Based on our calculation, coherent interfaces may form when the lattice misfit is between -0.0012-0.0146, whereas a semi-coherent interface may exist for lattice misfits as high as -0.0986 and 0.0228. Cubic YSZ films are susceptible to rupture beyond these lattice misfit values. A compressive stress as high as

2.33 GPa is predicted in a 5 nm thick c-YSZ film after incorporating the effect of lattice misfit of 0.0057 for a $(001)_{c-YSZ}$ // $(001)_{MCrAlY}$ and $[010]_{c-YSZ}$ // $[110]_{MCrAlY}$ coherent interface, as compared to -879 MPa of stress arising only due to thermal mismatch. An orientation relationship between film and substrate that results in a higher predicted stress than the fracture strength of the film may not be favorable for the formation of an interface. Hence the effect of lattice misfit should be considered while selecting the candidate materials for a TBC system. The degree of coherency decreases with increasing lattice misfit and film thickness. The stress within the film due to lattice misfit decreases with increasing film thickness and eventually only thermal stress remains within the film. However, dislocations nucleate at the metal-ceramic interface to reduce the interfacial adhesion. This condition results in a susceptibility to interfacial delamination of film at high film thicknesses.

ACKNOWLEDGEMENTS

This technical effort was performed in support of the National Energy Technology Laboratory's ongoing gasification research, in the Advance Reaction Systems program. This research was also supported in part by an appointment to the National Energy Technology Laboratory Research Participation Program, sponsored by the U.S. Department of Energy and administered by the Oak Ridge Institute for Science and Education.

DISCLAIMER

This work was funded by the U.S. Department of Energy, National Energy Technology Laboratory, an agency of the United States Government. Neither the United States Government

nor any agency thereof, nor any of their employees, makes any warranty, expressed or implied, or assumes any legal liability or responsibility for the accuracy, completeness, or usefulness of any information, apparatus, product, or process disclosed, or represents that its use would not infringe privately owned rights. Reference herein to any specific commercial product, process, or service by trade name, trademark, manufacturer, or otherwise, does not necessarily constitute or imply its endorsement, recommendation, or favoring by the United States Government or any agency thereof. The views and opinions of authors expressed herein do not necessarily state or reflect those of the United States Government or any agency thereof.

References

1. Burger, K., W. Mader, and M. Rühle, *Structure, chemistry and diffusion bonding of metal/ceramic interfaces.* Ultramicroscopy, 1987. **22**(1): p. 1-13.
2. Ohuchi, F.S. and M. Kohyama, *Electronic Structure and Chemical Reactions at Metal–Alumina and Metal–Aluminum Nitride Interfaces.* Journal of the American Ceramic Society, 1991. **74**(6): p. 1163-1187.
3. Liu, S.-S., et al., *Observation of the Ni/YSZ Interface in a Conventional SOFC*. Vol. 162. 2015. F750.
4. Howe, J.M., *Bonding, structure, and properties of metal/ceramic interfaces: Part 1 Chemical bonding, chemical reaction, and interfacial structure.* International Materials Reviews, 1993. **38**(5): p. 233-256.
5. Clarke, D.R., M. Oechsner, and N.P. Padture, *Thermal-barrier coatings for more efficient gas- turbine engines.* MRS Bulletin, 2012. **37**(10): p. 891-898.
6. Wang, C.-L., et al., *Synthesis of Gadolinium Zirconate by Coprecipitaiton and Its Properties for TBC Application.* Key Engineering Materials, 2005. **280-283**: p. 1501-1502.
7. Saini, A.K., D. Das, and M.K. Pathak, *Thermal Barrier Coatings -Applications, Stability and Longevity Aspects.* Procedia Engineering, 2012. **38**: p. 3173-3179.
8. Drexler, J.M., et al., *Thermal-gradient testing of thermal barrier coatings under simultaneous attack by molten glassy deposits and its mitigation.* Surface and Coatings Technology, 2010. **204**(16): p. 2683-2688.
9. Kumar, V. and K. Balasubramanian, *Progress update on failure mechanisms of advanced thermal barrier coatings: A review.* Progress in Organic Coatings, 2016. **90**: p. 54-82.
10. Josell, D., et al., *Heat transfer through nanoscale multilayered thermal barrier coatings at elevated temperatures.* Surface and Coatings Technology, 2015. **275**: p. 75-83.
11. Chawla, K.K., *Composite materials: science and engineering*. 2012: Springer Science & Business Media.

12. Howe, J.M., *Bonding, Structure and Properties of Metal/Ceramic Interfaces.* MRS Proceedings, 2011. **314**.
13. Qian, G., T. Nakamura, and C.C. Berndt, *Effects of thermal gradient and residual stresses on thermal barrier coating fracture.* Mechanics of Materials, 1998. **27**(2): p. 91-110.
14. Song, Y., et al., *Thermal Stress in Fabrication of Thermal Barrier Coatings.* Journal of Thermal Stresses, 2014. **37**(12): p. 1390-1415.
15. Martena, M., et al., *Modelling of TBC system failure: Stress distribution as a function of TGO thickness and thermal expansion mismatch.* Engineering Failure Analysis, 2006. **13**(3): p. 409- 426.
16. Białas, M., *Finite element analysis of stress distribution in thermal barrier coatings.* Surface and Coatings Technology, 2008. **202**(24): p. 6002-6010.
17. Hsueh, C.H., *Thermal stresses in elastic multilayer systems.* Thin Solid Films, 2002. **418**(2): p. 182-188.
18. Guo, C.Q., et al., *Predicting multilayer film's residual stress from its monolayers.* Materials & Design, 2016. **110**: p. 858-864.
19. Freund, L.B. and S. Suresh, *Thin film materials: stress, defect formation and surface evolution*. 2004: Cambridge University Press.
20. Wunderlich, W., *The Atomistic Structure of Metal/Ceramic Interfaces Is the Key Issue for Developing Better Properties.* Metals, 2014. **4**(3): p. 410.
21. Sillassen, M., et al., *Low-Temperature Superionic Conductivity in Strained Yttria-Stabilized Zirconia.* Advanced Functional Materials, 2010. **20**(13): p. 2071-2076.
22. Poklad, A., et al., *Orientation Relationship between the TRIP Steel Substrate and the ZrO2 thin Film.* steel research international, 2011. **82**(9): p. 985-989.
23. Dumin, D.J., *Deformation of and Stress in Epitaxial Silicon Films on Single-Crystal Sapphire.* Journal of Applied Physics, 1965. **36**(9): p. 2700-2703.
24. Englert, T., G. Abstreiter, and J. Pontcharra, *Determination of existing stress in silicon films on sapphire substrate using Raman spectroscopy.* Solid-State Electronics, 1980. **23**(1): p. 31-33.
25. Wang, Q.-Y., et al., *Characterization of stress induced in SOS and Si/γ-Al2O3/Si heteroepitaxial thin films by Raman spectroscopy.* Journal of Crystal Growth, 2005. **280**(1): p. 222-226.
26. Vreeland, T. and B.M. Paine, *X-ray diffraction characterization of multilayer semiconductor structures.* Journal of Vacuum Science & Technology A: Vacuum, Surfaces, and Films, 1986. **4**(6): p. 3153-3159.
27. Jain, S.C., A.H. Harker, and R.A. Cowley, *Misfit strain and misfit dislocations in lattice mismatched epitaxial layers and other systems.* Philosophical Magazine A, 1997. **75**(6): p. 1461- 1515.
28. Atkinson, A. and S.C. Jain, *The energy of systems of misfit dislocations in epitaxial strained layers.* Thin Solid Films, 1992. **222**(1): p. 161-165.
29. Kikuchi, A., *Calculation of Misfit-Dislocation Density Generated by Lattice Mismatch at the NiSi2– Si Interface.* physica status solidi (b), 1997. **203**(1): p. 79-86.
30. Willis, J.R., S.c. Jain, and R. Bullough, *The energy of an array of dislocations: Implications for strain relaxation in semiconductor heterostructures.* Philosophical Magazine A, 1990. **62**(1): p. 115-129.
31. Matthews, J.W. and A.E. Blakeslee, *Defects in epitaxial multilayers.* Journal of Crystal Growth, 1974. **27**: p. 118-125.
32. Matthews, J.W., *Defects associated with the accommodation of misfit between crystals.* Journal of Vacuum Science and Technology, 1975. **12**(1): p. 126-133.
33. Mazur, Z., et al., *Failure analysis of a gas turbine blade made of Inconel 738LC alloy.* Engineering Failure Analysis, 2005. **12**(3): p. 474-486.

34. Moridi, A., et al., *Residual stresses in thin film systems: Effects of lattice mismatch, thermal mismatch and interface dislocations.* International Journal of Solids and Structures, 2013. **50**(22): p. 3562-3569.
35. Linghu, Y., et al., *The Adhesive Properties of Coherent and Semicoherent NiAl/V Interfaces Within the Peierls-Nabarro Model.* Crystals, 2016. **6**(4): p. 32.
36. Aruna, S.T., N. Balaji, and K.S. Rajam, *Phase transformation and wear studies of plasma sprayed yttria stabilized zirconia coatings containing various mol% of yttria.* Materials Characterization, 2011. **62**(7): p. 697-705.
37. Chen, T., et al., *Phase stability, microstructural evolution and room temperature mechanical properties of TiO2 doped 8mol% Y2O3 stabilized ZrO2 (8Y-CSZ).* Ceramics International, 2008. **34**(2): p. 365-370.
38. Tabor, D., *The hardness of solids.* Review of Physics in Technology, 1970. **1**(3): p. 145.
39. Adams, J.W., R. Ruh, and K.S. Mazdiyasni, *Young's Modulus, Flexural Strength, and Fracture of Yttria-Stabilized Zirconia versus Temperature.* Journal of the American Ceramic Society, 1997. **80**(4): p. 903-908.
40. Jarvis, E.A. and E.A. Carter, *The Role of Reactive Elements in Thermal Barrier Coatings.* Computing in Science & Engineering, 2002. **4**(2): p. 33-41.
41. Christensen, A. and E.A. Carter, *Adhesion of ultrathin ZrO2(111) films on Ni(111) from first principles.* The Journal of Chemical Physics, 2001. **114**(13): p. 5816-5831.
42. Sasaki, T., et al., *Atomic and Electronic Structures of Ni/YSZ(111) Interface.* MATERIALS TRANSACTIONS, 2004. **45**(7): p. 2137-2143.
43. Dickey, E.C., et al., *Preferred crystallographic orientation relationships of nickel films deposited on (100) cubic-zirconia substrates.* Thin Solid Films, 2000. **372**(1): p. 37-44.
44. Heo, Y.-U., et al., *Oxidation and reduction behavior of Ni and NiO layers sputter deposited onto yttrium-stabilized zirconia single crystals.* Thin Solid Films, 2011. **520**(1): p. 138-143.
45. Tanaka, M., et al., *Residual stress measurement of an EB-PVD Y2O3-ZrO2 thermal barrier coating by micro-Raman spectroscopy.* Surface and Coatings Technology, 2009. **204**(5): p. 657-660.
46. Teixeira, V., et al., *Effects of deposition temperature and thermal cycling on residual stress state in zirconia-based thermal barrier coatings.* Surface and Coatings Technology, 1999. **120–121**: p. 103-111.
47. Li, C., et al., *Understanding the residual stress distribution through the thickness of atmosphere plasma sprayed (APS) thermal barrier coatings (TBCs) by high energy synchrotron XRD; digital image correlation (DIC) and image based modelling.* Acta Materialia, 2017. **132**: p. 1-12.
48. Vaßen, R., S. Giesen, and D. Stöver, *Lifetime of Plasma-Sprayed Thermal Barrier Coatings: Comparison of Numerical and Experimental Results.* Journal of Thermal Spray Technology, 2009. **18**(5): p. 835.
49. Dong, H., et al., *Effect of TGO Thickness on Thermal Cyclic Lifetime and Failure Mode of Plasma-Sprayed TBCs.* Journal of the American Ceramic Society, 2014. **97**(4): p. 1226-1232.
50. Lipkin, D.M., et al., *Stress development in alumina scales formed upon oxidation of (111) NiAl single crystals.* Corrosion Science, 1997. **39**(2): p. 231-242.
51. Thornton, J., S. Slater, and J. Almer, *The Measurement of Residual Strains Within Thermal Barrier Coatings Using High-Energy X-Ray Diffraction.* Journal of the American Ceramic Society, 2005. **88**(10): p. 2817-2825.
52. Kim, D.J., *Lattice Parameters, Ionic Conductivities, and Solubility Limits in Fluorite-Structure MO2 Oxide [M = Hf4+, Zr4+, Ce4+, Th4+, U4+] Solid Solutions.* Journal of the American Ceramic Society, 1989. **72**(8): p. 1415-1421.

53. Mishima, Y., S. Ochiai, and T. Suzuki, *Lattice parameters of Ni(γ), Ni3Al(γ') and Ni3Ga(γ') solid solutions with additions of transition and B-subgroup elements.* Acta Metallurgica, 1985. **33**(6): p. 1161-1169.
54. Ochial, S., Y. Oya, and T. Suzuki, *Alloying behaviour of Ni3Al, Ni3Ga, Ni3Si and Ni3Ge.* Acta Metallurgica, 1984. **32**(2): p. 289-298.